NETWORKS AND HETEROGENEOUS MEDIA
©American Institute of Mathematical Sciences
Volume **4**, Number **2**, June **2009**

doi:10.3934/nhm.2009.4.189

pp. **189–210**

METHODS FOR THE LOCALIZATION OF A LEAK IN OPEN WATER CHANNELS

Nadia Bedjaoui and Erik Weyer

Department of Electrical and Electronic Engineering, University of Melbourne
Parkville, VIC 3010, Australia

Georges Bastin

Center for Systems Engineering and Applied Mechanics (CESAME)
Department of Mathematical Engineering, Université catholique de Louvain
4, Avenue G. Lemaître, 1348 Louvain-la-Neuve, Belgium

Abstract. In this paper, we present two methods for determining the position of a leak in an open water channel. The available measurements are the water level and the gate position at the upstream and downstream end of a channel reach. We assume that the size of the leak and the time it started are already estimated by a leak-detection method. Both of the proposed methods make use of a nonlinear Saint-Venant equation model of the channel where the leak is modelled as a lateral outflow. The first method makes use of a bank of N models corresponding to N possible positions of the leak along the channel. The estimated position of the leak is determined by the model which minimizes a quadratic cost function. The second method is based on the same principle except that it uses observers instead of pure models. The methods are tested on both real and simulated data from the Coleambally Channel 6 in Australia. It is further shown that the determination of the position of a leak is an inherently difficult problem.

1. **Introduction.** Water is becoming an increasingly scarce resource in many parts of the world, and agriculture is one of the biggest consumers of water [13]. Water for agricultural purposes is often conveyed via a network of open channels. Management of such channels must take into account the required level of service that has to be provided to the farmers and the need to conserve water and minimize potential water losses. Implementation of automatic control systems for regulation of the flows and water levels ([6], [8], [9], [10], [11], [12], [14], [16], [17]) can give significant improvement in operational efficiency, ensuring that enough water is available to farmers while minimizing losses due to oversupply which can cause spillage along the channel and outflows at the end of the channel system.

In addition to losses caused by oversupply of water, there are also losses due to leaks in the channels [4],[18]. Leaks can e.g. occur in the form of unscheduled offtakes of water or be due to break downs and failures in the (often old) civil engineering infrastructure. A typical example is a gate to an escape channel not sealing properly and letting water through even when it is fully closed.

2000 *Mathematics Subject Classification.* Primary: 35L40, 35B37; Secondary: 93C95.

Key words and phrases. Hyperbolic partial differential equations, Saint-Venant equations, Observer design, Open water channels, Leak localization.

The research of the first and second author was supported by Rubicon Systems Australia and the Australian Research Council under the Linkage Grant Scheme, Project LP0349134.

Algorithms for leak detection based on simple lumped mass balance models were derived in [18], and the algorithms showed good performance when tested on an operational irrigation channel. In addition to detecting the presence of a leak, it is also of interest to estimate the location of the leak. Reaches in irrigation channels can be many kilometers long, and the time maintenance crew spend on localizing a leak can be reduced if an estimate of the likely location is provided.

In this paper we present two methods for leak localization. We assume that the leak has been detected and its size estimated, e.g. using methods from [18]. In view of the experimental results in that paper this is a reasonable assumption. Unlike algorithms for leak detection, methods for leak localization require a model involving the spatial variable. The main idea behind the developed methods is quite simple. We implement a bank of open loop models (Method 1) or observers (Method 2), and compare the output of the models/observers to the real measured water levels. Each model/observer corresponds to a particular leak location, and the leak location for the model/observer which minimizes a quadratic cost function of the error between the real water level and the water level computed by the model/observer is chosen as the estimated leak location.

The methods work well under ideal conditions, and some uncertainty can also be tolerated with only minor performance degradation. In any real world application the sensors will have finite precision and there will be mismatch between the real system and the models used for design, and under such conditions an analysis shows that the localization of leaks based on measurements at the upstream and downstream boundary of the channel reach is an inherently difficult problem.

The paper is organized as follows. In the next section we introduce the Saint-Venant equation models of the irrigation channel. In Section 3 we introduce the observer design and the methods for leak localization are described in Section 4. Simulation results and experimental results are given in Section 5. Section 6 presents an analysis of the inherent performance limitations before conclusions are given.

2. Model.

2.1. Channel description.

Figure 1 shows a sketch of a reach of a typical (Australian) irrigation channel of length L. The channel is automated with overshot gates, and the stretch between two gates is referred to as a pool or a reach. The water level is denoted by $Y(t,x)$ where t is the time variable and x is the spatial variable. We have measurements of the water levels at the upstream and downstream end, i.e. $Y(t,0)$ and $Y(t,L)$. The gate positions $p_0(t)$ and $p_L(t)$ can be imposed, which means that we can impose the flows $Q(t,0)$ and $Q(t,L)$ over the upstream and downstream gates respectively, since they are (assuming free flow conditions) given by [5]

$$Q(t,0) = c_0(Y_{\text{ups}}(t) - p_0(t))^{3/2} \tag{1}$$

$$Q(t,L) = c_L(Y(t,L) - p_L(t))^{3/2} \tag{2}$$

where Y_{ups} is the water level upstream of the upstream gate, and c_0 and c_L are known proportionality constants.

The gates are moved by electric motors, and power is supplied by solar panels. Data communication takes place via a radio network, and at each gate there is a micro-processor which can processes local information and information communicated over the radio network.

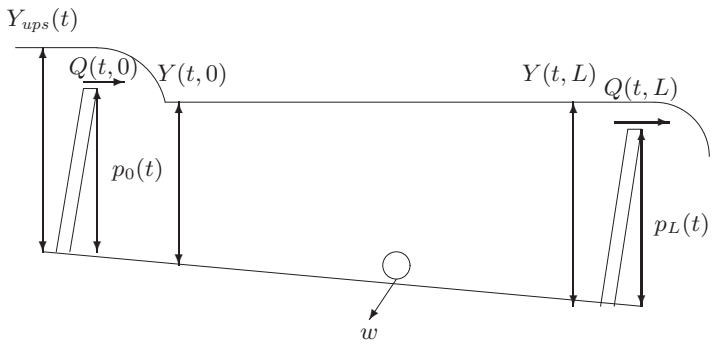

FIGURE 1. Schematic of a pool

2.2. **Model.** Assuming one-dimensional flow, the system can be modelled by the Saint-Venant equations which are a two coupled quasilinear hyperbolic Partial Differential Equations (PDE) representing a mass and a momentum balance. The dependent variables are the flow Q and the cross-sectional area A, and the independent variables are time t and the spatial variable x. For a channel with constant geometry, the Saint-Venant equations are given by

$$\partial_t \begin{pmatrix} A \\ Q \end{pmatrix} + F(A,Q)\partial_x \begin{pmatrix} A \\ Q \end{pmatrix} = H(A,Q,w) \tag{3}$$

$$F(A,Q) = \begin{pmatrix} 0 & 1 \\ gA\partial_A Y - \frac{Q^2}{A^2} & 2\frac{Q}{A} \end{pmatrix}$$

$$H(A,Q,w) = \begin{pmatrix} w \\ gA(S-S_f) + k_w \frac{Q}{A} w \end{pmatrix}$$

where ∂_t, ∂_x and ∂_A denote the partial derivatives with respect to time, spatial variable and cross-sectional area respectively. S is the bottom slope, g is the acceleration of gravity, $S_f = \frac{Q^2 n^2}{A^2 R(A)^{4/3}}$ is the friction slope, where n is the Manning coefficient and $R(A)$ is the hydraulic radius. w is the lateral outflow per unit length, and $k_w = 1$ for outflows ($w < 0$) and $k_w = 0$ for inflows ($w > 0$). In the rest of the paper we will assume $w \leq 0$ and hence $k_w = 1$. We assume that the outflow is uniform and limited to a small portion of the channel.

$$w(t,x) = \begin{cases} w(t) & l_i \leq x \leq l_{i+1} \\ 0 & \text{otherwise} \end{cases}$$

We will refer to this as a leak at location $x_i = (l_{i+1} + l_i)/2$. The initial conditions are given by

$$Q(0,x) = Q_0(x), \quad Y(0,x) = Y_0(x)$$

and the boundary conditions are

$$Q(t,0) = c_0(Y_{\text{ups}}(t) - p_0(t))^{3/2}, \quad \text{and} \quad Q(t,L) = c_L(Y(t,L) - p_L(t))^{3/2}$$

A PDE of the form (3) is called hyperbolic if the matrix F has real eigenvalues. For the Saint-Venant equations the eigenvalues are given by

$$\lambda_\pm = \frac{Q}{A} \pm \sqrt{gA\partial_A Y}$$

which for irrigation channels in subcritical flow are real with opposite sign, i.e. $\lambda_- < 0 < \lambda_+$.

3. **Observer.** The purpose of an observer is to reconstruct the state of a system from measurements of the inputs and outputs of the system. In the following we propose an observer to estimate the cross-sectional area $A(t,x)$ and the flow $Q(t,x)$ using the input measurements (upstream flow $Q(t,0)$ computed from (1), downstream gate position $p_L(t)$) and the output measurements (upstream and downstream water levels $Y(t,0)$ and $Y(t,L)$). The ideas behind the observer design are as follows:

First, the estimation problem is formulated as a control problem. The control objective is to regulate (A,Q) to an equilibrium $(\bar{A},\bar{Q})$ using the boundary condition $Q(t,0)$ and $Q(t,L)$ as inputs. The estimation problem is considered as a control problem where the objective is to regulate the estimation errors $(A-\hat{A},\, Q-\hat{Q})$ to $(0,0)$ by adjusting the estimation errors on the boundary. $\hat{A}$ and $\hat{Q}$ are the cross-sectional area and flow computed by the observer. In order to design the boundary conditions we appeal to the following recent results in control of irrigation channels.

In [10], it was shown that imposing boundary control of the form

$$\frac{Q(t,0)}{A(t,0)} = \frac{\bar{Q}(t,0)}{\bar{A}(t,0)} + \frac{1-k_0}{1+k_0}(\varphi(A(t,0)) - \varphi(\bar{A}(t,0))) \tag{4}$$

and

$$\frac{Q(t,L)}{A(t,L)} = \frac{\bar{Q}(t,L)}{\bar{A}(t,L)} - \frac{1-k_L}{1+k_L}(\varphi(A(t,L)) - \varphi(\bar{A}(t,L))) \tag{5}$$

with $0<k_0<1$ and $0<k_L<1$ and φ such that $\partial_A\varphi = \frac{\sqrt{gA\partial_A Y}}{A} > 0$ achieves the control objective for a horizontal, rectangular channel without friction and in the absence of offtakes ($H(A,Q,w)=0$).

In [2], it was further shown based on stability analysis of the linearized Saint-Venant equations in subcritical flow, that the boundary conditions of the form (4) and (5) are sufficient to regulate a rectangular non-horizontal channel with friction in the absence of offtakes.

The results were further extended in [15], where it was proved that the same boundary conditions can control a horizontal channel with friction and in the presence of offtakes which do not affect the momentum conservation.

3.1. **Proposed observer.** The proposed observer is of the form

$$\partial_t \begin{pmatrix} \hat{A} \\ \hat{Q} \end{pmatrix} + F(\hat{A},\hat{Q})\partial_x \begin{pmatrix} \hat{A} \\ \hat{Q} \end{pmatrix} = H(\hat{A},\hat{Q},\hat{w}) \tag{6}$$

$$F(\hat{A},\hat{Q}) = \begin{pmatrix} 0 & 1 \\ g\hat{A}\partial_{\hat{A}}\hat{Y} - \frac{\hat{Q}^2}{\hat{A}^2} & 2\frac{\hat{Q}}{\hat{A}} \end{pmatrix}$$

$$H(\hat{A},\hat{Q},\hat{w}) = \begin{pmatrix} \hat{w} \\ g\hat{A}(S-\hat{S}_f) + k_w\frac{\hat{Q}}{\hat{A}}\hat{w} \end{pmatrix}$$

with the initial conditions

$$\hat{Q}_0(x), \hat{A}_0(x)$$

$\hat{S}_f$ is the estimate of the friction slope computed using $\hat{A}$ and $\hat{Q}$, and $\hat{w}$ is an estimate of the outflow. For this observer we impose boundary conditions of the same form as in (4) and (5), i.e.

$$\frac{\hat{Q}(t,0)}{\hat{A}(t,0)} = \frac{Q(t,0)}{A(t,0)} + \frac{1-k_0}{1+k_0}(\varphi(A(t,0)) - \varphi(\hat{A}(t,0))) \tag{7}$$

$$\frac{\hat{Q}(t,L)}{\hat{A}(t,0)} = \frac{Q(t,L)}{A(t,L)} - \frac{1-k_L}{1+k_L}(\varphi(A(t,L)) - \varphi(\hat{A}(t,L))) \tag{8}$$

$0 < k_0 < 1$ and $0 < k_L < 1$ are the design parameters and φ is given by $\partial_A \varphi = \frac{\sqrt{gA\partial_A Y}}{A} > 0$.

3.2. **Stability analysis of the observer.** The proposed observer is a hyperbolic PDE. The main property of this class of PDE is the existence of the Riemann coordinates which are useful for proving existence of solutions as well as analysis and design of control methods [15].

3.2.1. *Riemann coordinates.* We first consider the model (3) of the irrigation channel. The Riemann coordinates are the change of coordinates $\xi = \begin{pmatrix} \xi_+ \\ \xi_- \end{pmatrix}$ whose Jacobian

$$P = \begin{pmatrix} \frac{\partial \xi_+}{\partial A} & \frac{\partial \xi_+}{\partial Q} \\ \frac{\partial \xi_-}{\partial A} & \frac{\partial \xi_-}{\partial Q} \end{pmatrix}$$

diagonalizes the matrix F of the PDE (3) such that

$$F = P^{-1}\Lambda P \quad \text{where} \quad \Lambda = \begin{pmatrix} \lambda_+ & 0 \\ 0 & \lambda_- \end{pmatrix}$$

By definition we have

$$\partial_t \xi = P\partial_t \begin{pmatrix} A \\ Q \end{pmatrix}, \quad \partial_x \xi = P\partial_x \begin{pmatrix} A \\ Q \end{pmatrix}$$

Then, left multiplying (3) by P, we obtain

$$P\partial_t \begin{pmatrix} A \\ Q \end{pmatrix} + PP^{-1}\Lambda(\xi)P\partial_x \begin{pmatrix} A \\ Q \end{pmatrix} = PH(A,Q,w) \tag{9}$$

which can be expressed in the new coordinates by

$$\partial_t \xi + \Lambda(\xi)\partial_x \xi = h(\xi, w) \tag{10}$$

where $h(\xi, w) = PH(A, Q, w)$.

The matrix P which diagonalizes F is

$$P = \begin{pmatrix} -\frac{Q}{A^2} + \frac{\sqrt{gA\partial_A Y}}{A} & \frac{1}{A} \\ -\frac{Q}{A^2} - \frac{\sqrt{gA\partial_A Y}}{A} & \frac{1}{A} \end{pmatrix}$$

and the Riemann coordinates are

$$\begin{cases} \xi_+ = \frac{Q}{A} + \varphi(A) \\ \xi_- = \frac{Q}{A} - \varphi(A) \end{cases}$$

where φ is given by

$$\partial_A \varphi = \frac{\sqrt{gA\partial_A Y}}{A}$$

and thus

$$h(\xi,w)=\begin{pmatrix} g(S-S_f)+\frac{\sqrt{gA\partial_A Y}}{A}w \\ g(S-S_f)-\frac{\sqrt{gA\partial_A Y}}{A}w \end{pmatrix}$$

Similarly to the Saint-Venant model (3), we define the Riemann coordinates $\hat{\xi}=\begin{pmatrix}\hat{\xi}_+\\ \hat{\xi}_-\end{pmatrix}$ of the observer (6) as

$$\begin{cases}\hat{\xi}_+=\frac{\hat{Q}}{\hat{A}}+\varphi(\hat{A})\\ \hat{\xi}_-=\frac{\hat{Q}}{\hat{A}}-\varphi(\hat{A})\end{cases}$$

with the Jacobian $\hat{P}=\begin{pmatrix} -\frac{\hat{Q}}{\hat{A}^2}+\frac{\sqrt{g\hat{A}\partial_{\hat{A}}\hat{Y}}}{\hat{A}} & \frac{1}{\hat{A}}\\ -\frac{\hat{Q}}{\hat{A}^2}-\frac{\sqrt{g\hat{A}\partial_{\hat{A}}\hat{Y}}}{\hat{A}} & \frac{1}{\hat{A}}\end{pmatrix}$. In the new coordinates the observer is represented by

$$\partial_t\hat{\xi}+\Lambda(\hat{\xi})\partial_x\hat{\xi}=h(\hat{\xi},w) \tag{11}$$

3.2.2. *Linearized observer.* Assume $w(t,x)=\bar{w}(x)$. The steady-state solution of the Saint-Venant equations is the pair $(\bar{A},\bar{Q})$ which satisfies $\partial_t\begin{pmatrix}\bar{A}\\ \bar{Q}\end{pmatrix}=0$. From (3), it follows that

$$\partial_x\begin{pmatrix}\bar{A}\\ \bar{Q}\end{pmatrix}=F^{-1}(\bar{A},\bar{Q})H(\bar{A},\bar{Q},\bar{w}) \tag{12}$$

which gives

$$\partial_x\bar{Q} = \bar{w} \tag{13}$$

$$\partial_x\bar{A} = (g\bar{A}\partial_{\bar{A}}\bar{Y}-\frac{\bar{Q}^2}{\bar{A}^2})^{-1}(g\bar{A}(S-\bar{S}_f)-(2-k_w)\frac{\bar{Q}}{\bar{A}}\bar{w}) \tag{14}$$

The steady-state solution $(\bar{A},\bar{Q})$ corresponds to the pair $(\bar{\xi}_+=\frac{\bar{Q}}{\bar{A}}+\varphi(\bar{A}),\bar{\xi}_-=\frac{\bar{Q}}{\bar{A}}-\varphi(\bar{A}))$ in the Riemann coordinates which is a steady-state solution of (10) satisfying $\partial_t\bar{\xi}=0$ and $\partial_x\bar{\xi}=\Lambda^{-1}(\bar{\xi})h(\bar{\xi})$.

To linearize a function $g(\xi,w)$ around the steady-state $(\bar{\xi},\bar{w})$ of (10), we use the Taylor approximation

$$g(\xi,w)=g(\bar{\xi},\bar{w})+\frac{\partial g}{\partial\xi}|_{(\bar{\xi},\bar{w})}(\xi-\bar{\xi})+\frac{\partial g}{\partial w}|_{(\bar{\xi},\bar{w})}(w-\bar{w})$$

Let $\alpha=\xi-\bar{\xi}$ and $\bar{w}=0$. The linearization of (10) gives

$$\partial_t\alpha(t,x)+C(\bar{\xi})\partial_x\alpha(t,x)=B(\bar{\xi})\alpha(t,x)+W(\bar{\xi})w(t,x) \tag{15}$$

where $C(\bar{\xi})=\Lambda(\bar{\xi})$, $B(\bar{\xi})=\partial_\xi h(\bar{\xi})$ and $W(\bar{\xi})=\lim_{w\to0^-}\partial_w h(\bar{\xi})$. In the same way, we linearize the observer around the same steady-state $\bar{\xi}$ and we obtain

$$\partial_t\hat{\alpha}(t,x)+C(\bar{\xi})\partial_x\hat{\alpha}(t,x)=B(\bar{\xi})\hat{\alpha}(t,x)+W(\bar{\xi})\hat{w}(t,x) \tag{16}$$

where $\hat{\alpha}=\hat{\xi}-\bar{\xi}$ and $C(\bar{\xi})$, $B(\bar{\xi})$ and $W(\bar{\xi})$ are given above. In the original coordinates α and $\hat{\alpha}$ are given by

$$\alpha=\begin{pmatrix}\alpha_+\\ \alpha_-\end{pmatrix}=\begin{pmatrix}\frac{Q}{A}-\frac{\bar{Q}}{\bar{A}}+(\varphi(A)-\varphi(\bar{A}))\\ \frac{Q}{A}-\frac{\bar{Q}}{\bar{A}}-(\varphi(A)-\varphi(\bar{A}))\end{pmatrix} \tag{17}$$

$$\hat{\alpha} = \begin{pmatrix} \hat{\alpha}_+ \\ \hat{\alpha}_- \end{pmatrix} = \begin{pmatrix} \frac{\hat{Q}}{\hat{A}} - \frac{\bar{Q}}{\bar{A}} + (\varphi(\hat{A}) - \varphi(\bar{A})) \\ \frac{\hat{Q}}{\hat{A}} - \frac{\bar{Q}}{\bar{A}} - (\varphi(\hat{A}) - \varphi(\bar{A})) \end{pmatrix} \tag{18}$$

3.2.3. *Convergence of estimation error.* Define the estimation error e in the Riemann coordinates as

$$e(t,x) = \alpha(t,x) - \hat{\alpha}(t,x)$$

Then

$$\partial_t e(t,x) = \partial_t \alpha(t,x) - \partial_t \hat{\alpha}(t,x)$$

and from (15) and (16) it follows that

$$\partial_t e(t,x) + C(\bar{\xi})\partial_x e(t,x) = B(\bar{\xi})e(t,x) + W(\bar{\xi})e_w(t,x) \tag{19}$$

where $e_w(t,x)$ is given by $e_w(t,x) = w(t,x) - \hat{w}(t,x)$. We now observe that the dynamics governing the estimation error are the same as in (15), and hence the stability results based on an analysis of a linearized model summarized in Section 3 carry over to the observer.

4. **Localization scheme.** Here, we present the two methods for determination of the position of the leak.

4.1. **Method based on the models.** In order to find the position of the leak, we consider N equidistant possible positions x_j of the leak along the channel. For each position x_j, we build a model of the type (3) where the leak is modelled as a lateral outflow at position x_j. We then form a bank of the N models as shown in Figure 2. The outputs Y_j of the models are then compared to the system output Y, and a quadratic cost function J is evaluated

$$J(x_j) = \int_t^{t+T} \left([Y(\sigma,0) - Y_j(\sigma,0,x_j)]^2 + [Y(\sigma,L) - Y_j(\sigma,L,x_j)]^2 \right) d\sigma, \quad j = 1,\dots,N \tag{20}$$

where T represents the time horizon. It is a design parameter and its selection is commented on the last section of the paper. Moreover, weights on the upstream and downstream quadratic water level error can also be introduced as design parameters. The estimated position of the leak is determined by the model which minimizes the cost function, i.e.

$$\hat{x}_l = \arg \min_{x_j,\ j=1,\dots,N} J(x_j)$$

4.2. **Method based on the observers.** The underlying principle for estimation of the position of the leak is the same. However, here we use observers instead of models. We design an observer of the form (6) for each position $x_j, j = 1,...,N$ of the leak and form a bank of N observers (Figure 3). Observers of this type have also been used for leak localization in pipelines, see [1].

As in the previous method, the observer outputs $\hat{Y}_j$ are compared to the system outputs using the cost function J

$$J(x_j) = \int_t^{t+T} \left([Y(\sigma,0) - \hat{Y}_j(\sigma,0,x_j)]^2 + [Y(\sigma,L) - \hat{Y}_j(\sigma,L,x_j)]^2 \right) d\sigma$$

The estimated leak position is as before given by

$$\hat{x}_l = \arg \min_{x_j,\ j=1,\dots,N} J(x_j)$$

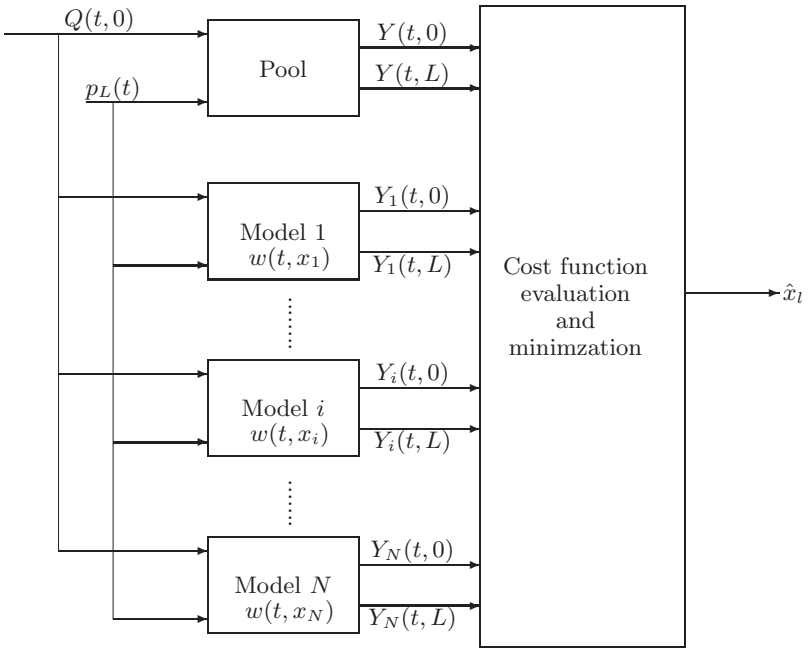

FIGURE 2. Bank of models

Figure 3 shows the bank of observers where f_0 and f_L denote the following boundary conditions

$$\begin{aligned} \hat{Q}(t,0) &= f_0(Q(t,0), A(t,0), \hat{A}(t,0)) \\ &= \tfrac{\hat{A}(t,0)}{A(t,0)} Q(t,0) + \tfrac{1-k_0}{1+k_0}(\varphi(A(t,0)) - \varphi(\hat{A}(t,0))) \end{aligned} \tag{21}$$

$$\begin{aligned} \hat{p}_L(t) &= f_L(p_L(t), Y(t,L), \hat{Y}(t,L)) \\ &= \hat{Y}(t,L) - \tfrac{1}{c_L}[\tfrac{\hat{A}(t,L)}{A(t,L)} Q(t,L) - \tfrac{1-k_L}{1+k_L}(\varphi(A(t,L)) - \varphi(\hat{A}(t,L)))]^{3/2} \end{aligned} \tag{22}$$

These boundary conditions are the same as those in Section 3.1, but expressed in terms of the upstream flow and the downstream gate position.

5. **Application.** In order to test the performance of the proposed methods on both simulated and real data, we considered Pool 4 of the Coleambally 6 channel which is an operational irrigation channel in Australia. The channel has a trapezoidal cross-section and hence the cross-sectional area is given by $A = (b + zY)Y$ where b is the bottom width and z is the side slope. The channel data are summarized in Table 1.

Note that the stability analysis of the observers in Section 3.2.3 does not cover this case since the channel is trapezoidal and the lateral outflows will of course affect both the mass and momentum balance. We have however chosen this example as it corresponds to a real irrigation pool.

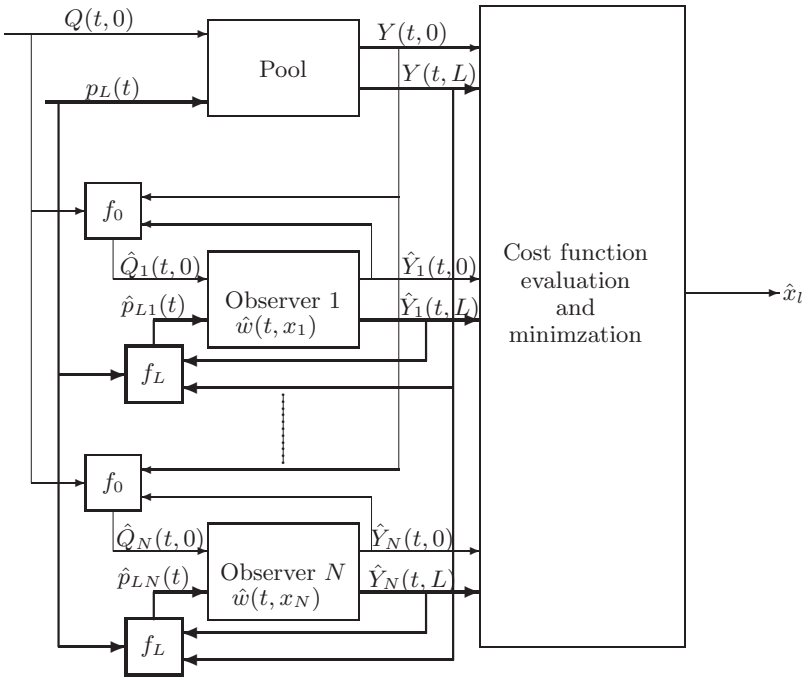

FIGURE 3. Bank of observers

Parameter	Symbol	Value	Dimension
Length	L	943	m
Bottom width	b	1.68	m
Side slope	z	2	
Bottom slope	S	$3.45 \cdot 10^{-4}$	
Downstream gate width	b_u	1.91	m
Normal water depth	y_n	1.5	m
Manning coefficient	n	0.02	
Sampling time	Δt	60	s
Gate coefficient	$c_L = (0.6 b_u \sqrt{g})$	3.58	$m^{-1/2} s^{-1}$

TABLE 1. Parameters for Pool 4

5.1. **Implementation.** To implement the methods, we use the numerical Preissmann scheme. It is a finite difference method for solving the Saint-Venant equations. The time t and the spatial variable x are discretized onto a grid on which the Saint-Venant equations are solved using approximations of the partial derivatives. In the Preissmann model, a variable f (in our case A, Q and w) and its derivatives are approximated as follows [7]

$$f = \frac{1}{2}\alpha(f_{i+1}^{k+1} + f_i^{k+1}) + \frac{1}{2}(1-\alpha)(f_{i+1}^{k} + f_i^{k})$$

$$\partial_t f = \frac{(f_i^{k+1} + f_{i+1}^{k+1}) - (f_i^k + f_{i+1}^k)}{2\Delta t}$$
$$\partial_x f = \frac{\alpha(f_{i+1}^{k+1} - f_i^{k+1}) + (1-\alpha)(f_{i+1}^k - f_i^k)}{\Delta x}$$

where the subscript $i = 0, ..., N$ denotes the spatial grid point and $k = 1, 2, ...$ denotes the time grid point. Δx and Δt are the grid intervals along the x-axis and t-axis respectively.

The above equations are augmented with the upstream ($i = 0$, corresponding to $x = 0$) and downstream boundary conditions ($i = N$, corresponding to $x = L$)

$$Q_{i=0}^{k+1} = Q((k+1)\Delta t, 0)$$
$$Q_{i=N}^{k+1} = c_L(Y_{i=N}^{k+1} - p_L((k+1)\Delta t))^{3/2}$$

For the simulations, we used $N = 50$ which is also the number of possible leak locations we considered along the channel. $\Delta x = L/N = 18.86m$ and $\Delta t = 60s$. Typical values of α are between 0.6 and 0.7 [7]. Here we used $\alpha = 0.6$. In the simulations, a leak is modelled as a uniform lateral outflow in section $s_i = [l_i, l_{i+1}]$ where $l_{i+1} = l_i + \Delta x, i = 1, N-1$ with $l_1 = 0$ and $l_N = L$. The position x_i of the leak is by convention taken as the midpoint of the section, i.e. $x_i = l_i + \frac{l_{i+1} - l_i}{2}$.

5.2. **Simulated data.** In this section we present simulation results which show

1. The performance of the observer and the effect of the gains k_0 and k_L on the speed of convergence
2. The performance of the leak localization methods in the ideal case (no model uncertainty, no measurement noise etc.)
3. The performance limitation of the methods in a real world scenario (model uncertainty, uncertainty in the size and start time of the leak etc.)

We consider the following scenario. The upstream flow and the downstream gate position are constant at $Q(t, 0) = \bar{Q} = 0.6m^3/s$ and $p_L(t) = \bar{p}_L = 1.35m$ as shown in Figure 4. A leak of size $0.2m^3/s$ starts at time $t_w = 200$ min in section number 35. The simulated upstream and downstream water levels are shown in Figure 5. In the beginning there is a transient before steady-state conditions are reached, and the water levels start decreasing at time 200 min when the leak occurred.

5.2.1. *Observer performance:* In order to illustrate the performance of the observer, the estimation errors $e(t, L) = Y(t, L) - \hat{Y}(t, L)$ are plotted in Figure 6 for the observer gains $k_0 = k_L = \{-0.01, -0.05, -0.1, -0.2\}$.

As we can see, the observers work very well also in this case when the channel is trapezoidal. The estimation error converges to zero, and the speed of convergence depends on the values k_0 and k_L. The convergence speed increases as $|k_0|, |k_L|$ decreases. The gains $k_0 = k_L = -0.01$ corresponding to the fastest convergence are used in the rest of the paper.

5.2.2. *Performance of the leak localization methods.* Here we demonstrate the ability of the two proposed methods to find the position of the leak. To this end we assume that $Y(t, 0)$ and $Y(t, L)$ in Figure 5 are the actual measurements and that the size of the leak and the time it starts are known and equal to the true values of $0.2m^3/s$ and 200 min. We consider 50 possible positions of the leak, each corresponding to an 18.86 meter section of the channel as used in the discretization of the models. We construct a bank of 50 models/observers, each one corresponding to a particular position(section) of the leak. The upper and lower integration limits

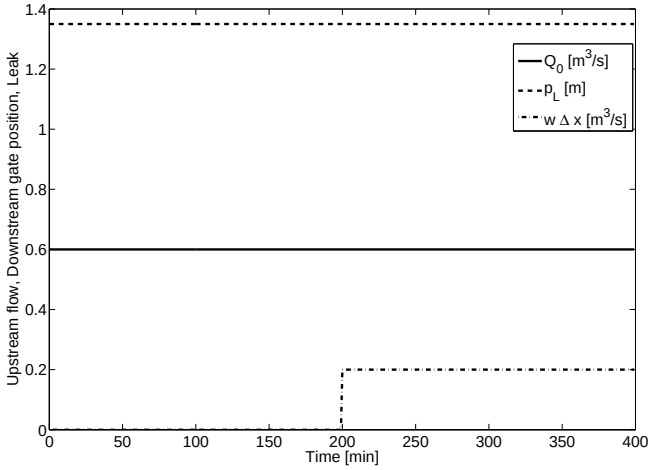

FIGURE 4. Input signals used in simulation

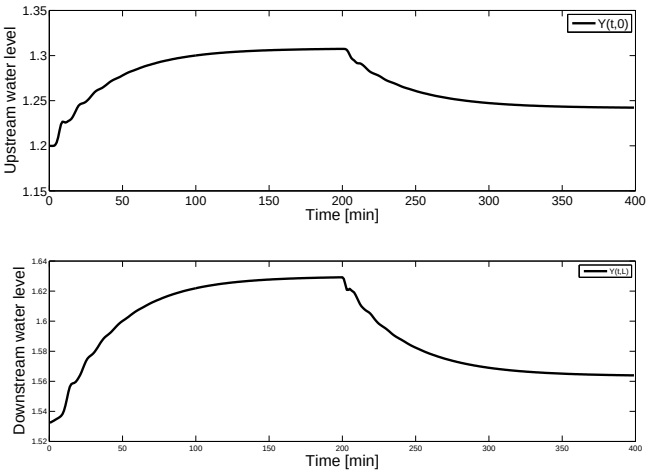

FIGURE 5. Upstream and downstream water level [m]

in the cost function J (equation 20) are 190 and 230 min respectively. The cost function is shown in Figure 7 for each one of the models/observers in the bank. We see that the cost functions for both methods attain their minima when the leak is correctly modelled as being in section no. 35, and hence the leak localization methods work under ideal condition. In practice however, the data are noisy, and the model is imperfect. Next we show the influence of uncertainty in the model parameter and uncertainty in the time the leak starts on the leak localization methods.

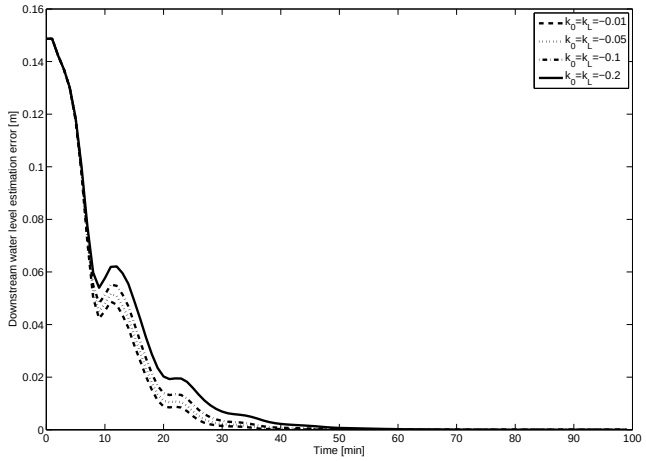

FIGURE 6. Estimation error in downstream water level computed with different observer gains

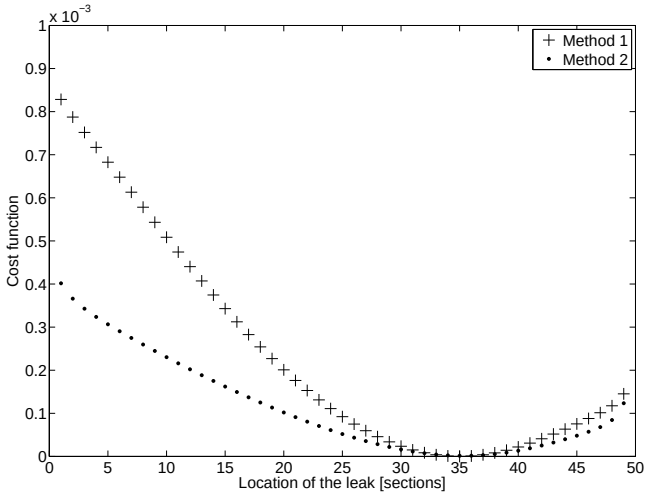

FIGURE 7. Cost functions J for the leak localization methods

5.2.3. *Limitations of the localization methods.* In practice, it is not required to pinpoint the position of the leak in the channel exactly and an error of ± 100 meters is often acceptable since the time it takes to physically locate the leak in the field will still be reduced. In the following we demonstrate the range of uncertainty that can be tolerated before the localization error becomes large. We first consider the presence of model uncertainty. Here, a range of Manning coefficient n in the interval $[0, 0.025]$ is used in the models/observers. Such change is realistic since there can be a difference in the friction at the beginning of the irrigation season when the channel is "clean" and at the end when it can be full of weeds. The cost functions

obtained for $n = 0$ and $n = 0.025$ are shown in Figure 8. For both methods, the obtained position of the leak is between section no. 30 and section no. 37. The true location of the leak is in section no. 35, and hence for the considered range of Manning coefficient, the error is between -94 meters and 37 meters since the sections are 18.8 meters long.

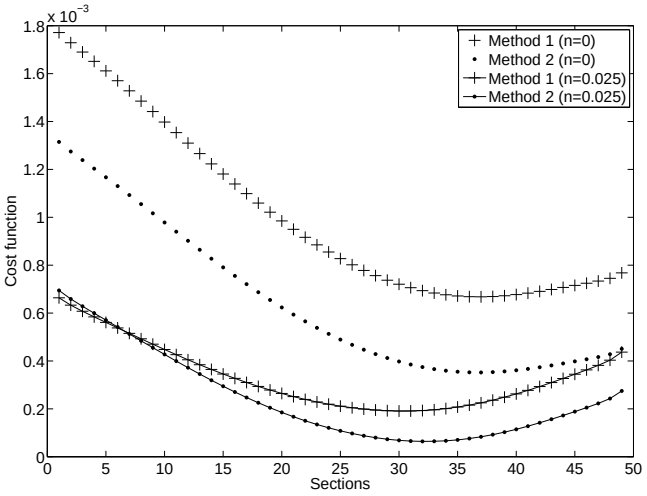

FIGURE 8. Cost functions J for the leak localization methods with model uncertainty

Next, we consider uncertainty in the start time of the leak t_w. In this simulation, the leak starts at different times than what is assumed i.e. $t_w = 198, 199, 201, 202$ minutes. The results in Figure 9 show that for $t_w = 198, 199$ and 201 the minima of the cost functions for both methods occur when the leak is modelled between section no. 30 and 40 which corresponds to errors between -94 meters and 94 meters. However, when the start time is 202 minutes, the leak location is given at section no. 25 (in the middle of the channel) which corresponds to 188 meters of error. Hence a small uncertainty of two minutes in the start time of the leak can lead to a relatively large error in the position. We will discuss this further in Section 6.

5.3. **Experimental data.** The data set shown in Figure 10 is from the Coleambally no. 6 channel. There is an offtake point to a farm just upstream of the downstream gate in Pool 4, and a water withdrawal started at that location at time 70 min. The CUSUM algorithm developed in [18] was applied to this data set, and the leak was detected at time 70 min which means that the algorithm provided an accurate estimate of the start time of the water withdrawal (see [18]). The estimated size of the leak $\hat{w}$ is shown in Figure 11 together with the measured value. This estimate will be used in the localization methods.

5.3.1. *Calibrated model.* In order to use a more accurate model and to reduce the effect of model uncertainties on the leak localization schemes, we first calibrated the parameters of the model to the real data. The calibrated parameters are the Manning coefficient $n = 0.05$ and the gate coefficient $c_L = 4$. Upstream and

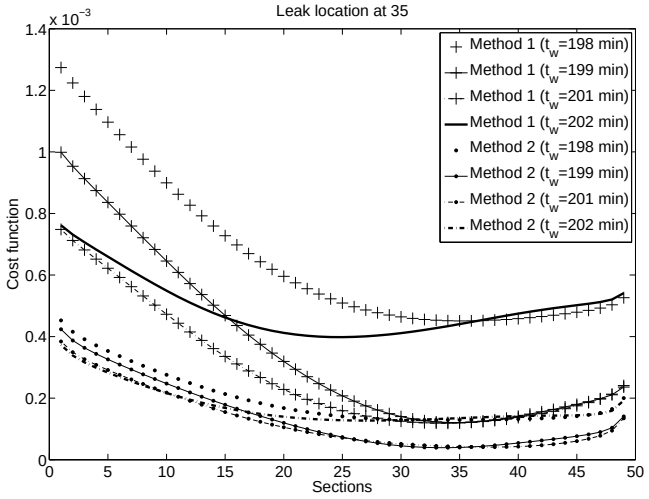

FIGURE 9. Cost functions J for the leak localization methods when the leak starts earlier or later than assumed

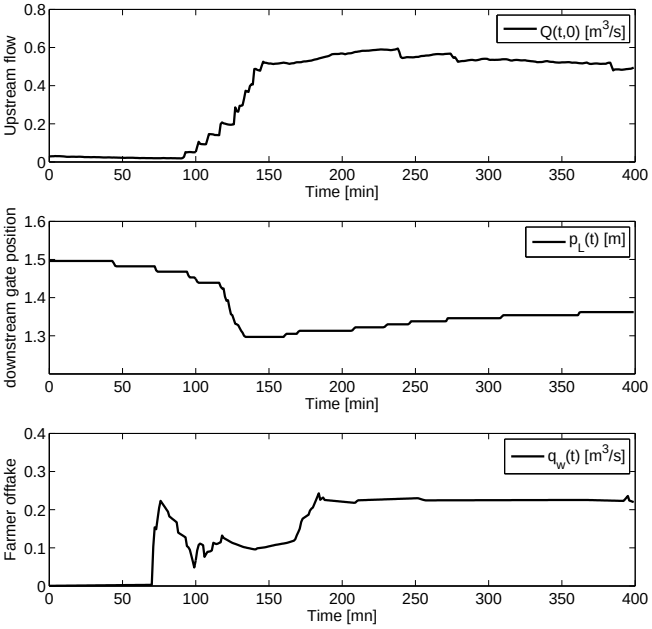

FIGURE 10. Inflow, downstream gate position and offtake from operational irrigation channel

downstream water levels generated with the calibrated model are shown together

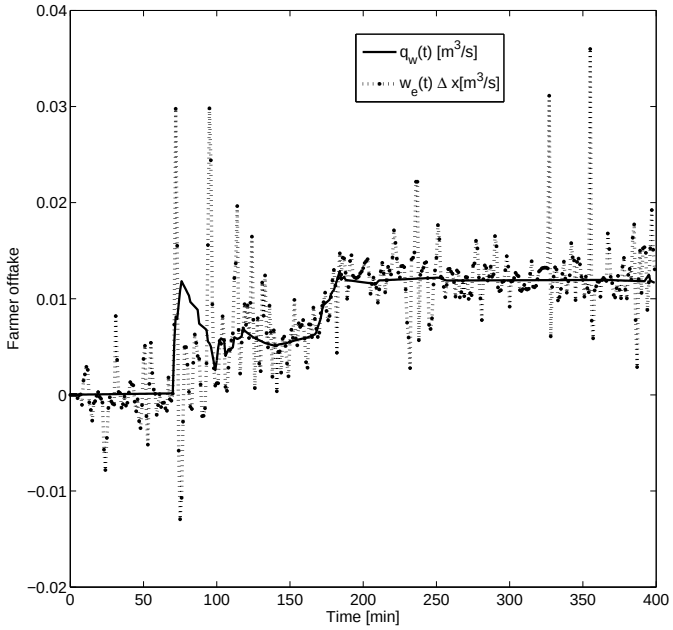

FIGURE 11. Measurement of the offtake and its estimated value

with the real data in Figure 12. As we can see, the model follows the real water levels well.

5.3.2. *Results with the leak localization methods.* From Figure 13, we see that both methods give a minimum of the cost function for section no. 33, i.e. they fail to find the right location of the leak which is in section 50.

From the obtained results it seems that the proposed localization methods are only performing well when there is limited uncertainty. Realistic uncertainties significantly affect the performance of the methods. In the next section, we will illustrate using a simple case study and the characteristic method for solutions of hyperbolic PDEs the difficulty of the leak localization problem.

6. **Discussion.** In this section, we consider the Saint-Venant model (3) expressed in the Riemann coordinates

$$\partial_t \begin{pmatrix} \xi_+ \\ \xi_- \end{pmatrix} + \begin{pmatrix} \lambda_+(\xi) & 0 \\ 0 & \lambda_-(\xi) \end{pmatrix} \partial_x \begin{pmatrix} \xi_+ \\ \xi_- \end{pmatrix} = \begin{pmatrix} h_+(\xi) \\ h_-(\xi) \end{pmatrix} + \begin{pmatrix} h_{w_+}(\xi, w) \\ h_{w_-}(\xi, w) \end{pmatrix} \quad (23)$$

where $\lambda_+ = \frac{Q}{A} + \sqrt{gA\partial_A Y}$, $\lambda_- = \frac{Q}{A} - \sqrt{gA\partial_A Y}$, $h_+ = h_- = g(S - S_f)$, $h_{w_+} = -h_{w_-} = \frac{\sqrt{gA\partial_A Y}}{A} w$. The available measurements are the upstream and downstream water levels and gate positions from which the Riemann coordinates $\xi(t, 0)$ and $\xi(t, L)$ can be computed.

6.1. **Characteristic method.** The principle of the characteristic method is to transform the PDE (23) into an equivalent set of ordinary differential equations

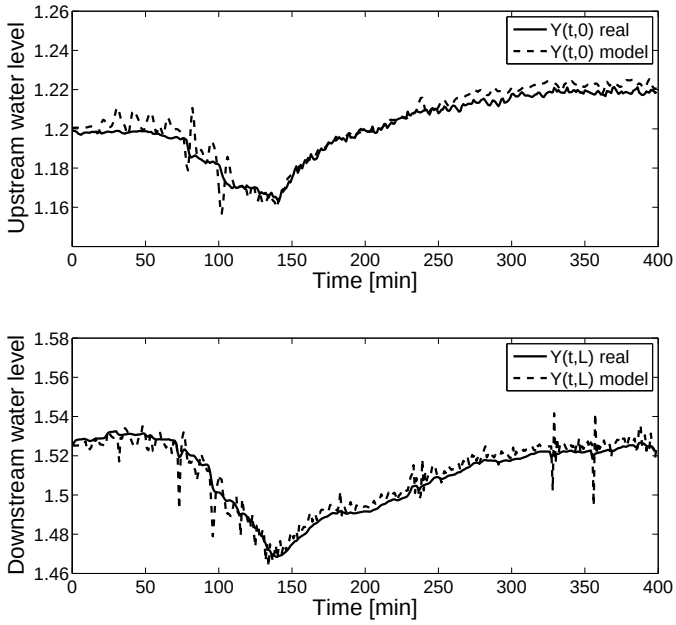

FIGURE 12. Calibrated model outputs and the measurements

(ODE). From the total derivatives $d\xi_+ = \frac{\partial \xi_+}{\partial t}dt + \frac{\partial \xi_+}{\partial x}dx$ and $d\xi_- = \frac{\partial \xi_-}{\partial t}dt + \frac{\partial \xi_-}{\partial x}dx$ it follows that

$$\frac{d\xi_+}{dt} = \frac{\partial \xi_+}{\partial t} + \frac{\partial \xi_+}{\partial x}\frac{dx}{dt} \tag{24}$$

$$\frac{d\xi_-}{dt} = \frac{\partial \xi_-}{\partial t} + \frac{\partial \xi_-}{\partial x}\frac{dx}{dt} \tag{25}$$

By imposing $\frac{d\xi_+}{dt} = h_+(\xi) + h_{w_+}(\xi, w)$ and $\frac{dx}{dt} = \lambda_+(\xi)$ in (24) and $\frac{d\xi_-}{dt} = h_-(\xi) + h_{w_-}(\xi, w)$ and $\frac{dx}{dt} = \lambda_-(\xi)$ in (25), the system (24)-(25) is equivalent to (23) and solving the PDE consists in solving the system of ODE

$$\begin{cases} \frac{d\xi_+}{dt} &= h_+(\xi) + h_{w_+}(\xi, w) \\ \frac{dx}{dt} &= \lambda_+(\xi) \end{cases} \tag{26}$$

$$\begin{cases} \frac{d\xi_-}{dt} &= h_-(\xi) + h_{w_-}(\xi, w) \\ \frac{dx}{dt} &= \lambda_-(\xi) \end{cases} \tag{27}$$

The solutions to the equations which only involve the independent variables are called the characteristic curves and the solutions to the equations involving the dependent variables are called the solution of the PDE along the characteristic. To illustrate the method, consider the case where $h_+ = h_- = 0$, $h_{w_+} = h_{w_-} = 0$ and $\lambda_+(\xi) = \bar{\lambda}_+$, $\lambda_-(\xi) = \bar{\lambda}_-$ constant. The system of ODE is reduced to

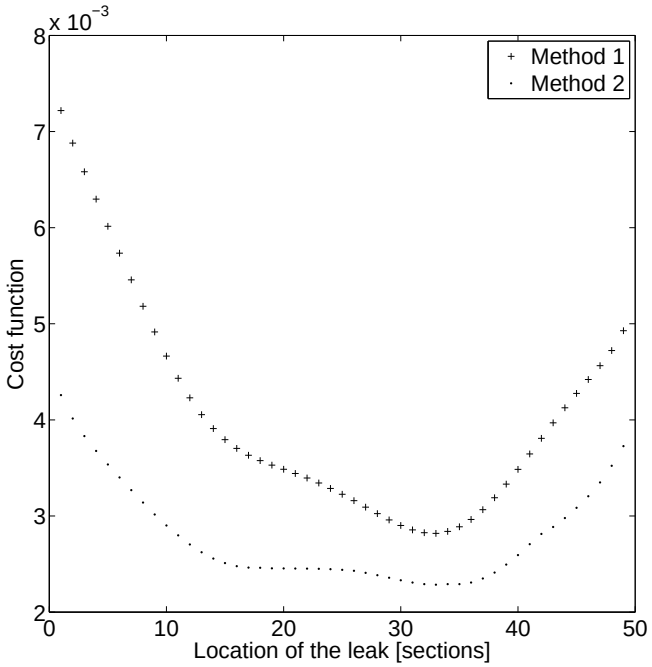

FIGURE 13. Cost function J with experimental data

$$\begin{cases} \frac{d\xi_+}{dt} &= 0 \\ \frac{dx}{dt} &= \bar{\lambda}_+ \end{cases} \tag{28}$$

$$\begin{cases} \frac{d\xi_-}{dt} &= 0 \\ \frac{dx}{dt} &= \bar{\lambda}_- \end{cases} \tag{29}$$

In this case, the characteristics are lines of slope $\bar{\lambda}_+ > 0$ corresponding to the positive characteristic C_+ and $\bar{\lambda}_- < 0$ corresponding to the negative characteristic C_-. Moreover, the solutions ξ_+ and ξ_- are constant along the characteristics C_+ and C_- respectively.

Figure 14 illustrates the solution in the (x,t) plane. There are two types of lines in the figure

- The solid lines corresponding to characteristics with initial values $(t=0, x=x_0)$ on the initial condition axis. These lines are defined by

$$C_+ : x(t) = \bar{\lambda}_+ t + x_0, \quad 0 \le t \le \frac{L - x_0}{\bar{\lambda}_+}$$

$$C_- : x(t) = \bar{\lambda}_- t + x_0, \quad 0 \le t \le \frac{x_0}{|\bar{\lambda}_-|}$$

  The solutions along these lines are constant and equal to the initial condition $\xi_+(t,x) = \xi_+(0,x_0)$ along C_+ and $\xi_-(t,x) = \xi_-(0,x_0)$ along C_-.
- The dashed lines correspond to characteristics with initial values $(t_c, x(t_c) = 0)$ and $(t_c, x(t_c) = L)$ on the boundary condition axes ($x = 0$ and $x = L$). These

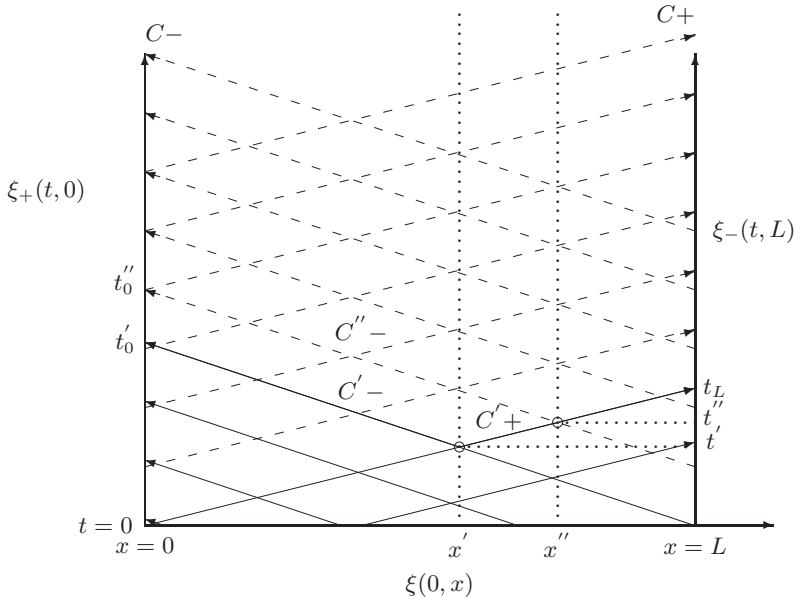

FIGURE 14. Characteristic method

characteristics are defined by the equations

$$C_+ : x(t) = \bar{\lambda}_+(t - t_c), \quad t_c \leq t \leq t_c + \frac{L}{\bar{\lambda}_+}$$

$$C_- : x(t) = \bar{\lambda}_-(t - t_c) + L, \quad t_c \leq t \leq t_c + \frac{L}{|\bar{\lambda}_-|}$$

The solutions along these lines are constant and equal to the boundary conditions $\xi_+(t,x) = \xi_+(t_c,0)$ along C_+ and $\xi_-(t,x) = \xi_-(t_c,L)$ along C_-.

To summarize, along a characteristic, the solution is determined either by the initial conditions or by the boundary conditions. The solution $\xi(t,x)$ is determined by the boundary condition for all $t \geq \frac{L}{\min(\lambda_+,|\lambda_-|)}$.

6.2. **Physical interpretation.** In subcritical flow, the solution to the Saint-Venant equations represents two coupled waves, one travelling downstream and one travelling upstream. The characteristic curves C_+ and C_- show how a wave originating at the point (t,x) propagates upstream and downstream. The eigenvalues $\bar{\lambda}_+ > 0$ and $\bar{\lambda}_- < 0$ are the velocities of the waves. Assume now that a constant leak of size w starts at time $t = t_1$ in position x_1, i.e. $h_{w_+}(\xi(x_1,t), w(x_1,t)) \neq 0$ and $h_{w_-}(\xi(x_1,t), w(x_1,t)) \neq 0$ for $t \geq t_1$. The system of ODE becomes

$$\frac{d\xi_+}{dt} = \frac{\sqrt{gA\partial_A Y}}{A} w(t,x) \tag{30}$$

$$\frac{dx}{dt} = \lambda_+(\xi) \tag{31}$$

and

$$\frac{d\xi_-}{dt} = -\frac{\sqrt{gA\partial_A Y}}{A} w(t,x) \tag{32}$$

$$\frac{dx}{dt} = \lambda_-(\xi) \tag{33}$$

where $\lambda_+ = \frac{Q}{A} + \sqrt{gA\partial_A Y}$ and $\lambda_- = \frac{Q}{A} - \sqrt{gA\partial_A Y}$.

It is clear from (31) and (33) that the presence of a leak w affects the solution ξ and therefore also the characteristics. The solution ξ and the velocities λ_+ and λ_- are no longer constant. Next we will heuristically argue that the leak localization problem is an inherently difficult problem, and in the process reveal the reasons for the difficulties. We make the following observations

1. The velocities $\lambda_+(\xi)$ and $\lambda_-(\xi)$ remain close to the constant values λ_+ and λ_-. The eigenvalues $\lambda_\pm$ are given by $\lambda_\pm = \frac{Q}{A} \pm \sqrt{gA\partial_A Y} = V \pm C$ where $V = \frac{Q}{A}$ is the average velocity of the water flow due to the kinetic energy and $C = \sqrt{gA\partial_A Y}$ is the celerity of waves due to the potential energy. In subcritical flows as typically seen in irrigation channels, C completely dominates V so $\lambda_+ \approx -\lambda_-$. (For the data in Figure 5, C is about 40 times the value of V.) That is the waves travel upstream and downstream with approximately the same speed. Moreover, for the changes in water levels and flows due to leaks as e.g. shown in Figure 5 and 12, the change in the value of C is less than 2 per cent and hence even with a leak the characteristic curves remain close to straight lines.
2. Leaks originating at different locations can have very similar effect at the downstream end. Assume that we have two leaks originating at (t', x') and (t'', x'') such that the effect reaches the downstream end at the same time t_L (see Figure 14). (From the above discussion it follows that both (t', x') and (t'', x'') are close to one of the straight lines $(C_+^{'})$ with slope λ_+.) The difference in $\xi_+(t, L)$ will be very small in any realistic scenario. The reason is that the change in ξ_+ comes from when (30) is integrated along the part of the characteristic where $w(t, x)$ is non-zero, and a translation of $w(t, x)$ along the characteristic only leads to a small change to the solution on the boundary. Hence it will be very difficult to distinguish a leak starting in position x' and time t' from a leak in position x'' starting at time t''. However, the effects will reach the upstream end at different times ($t_0^{'}$ and $t_0^{''}$) since (t', x') and (t'', x'') will be on different characteristics $C_-^{'}$ and $C_-^{''}$. As the velocities λ_+ and λ_- are typically in the order of several meters per second (around $3m/s$ for the data in Figure 5 and 12), the above observations indicates that leak localization is an inherently difficult problem since essentially only data observed in a narrow time frame at the upstream end and downstream end allows us to discriminate between leak locations.

As an example, consider the same scenario as in Section 5.2.2 with data given in Figure 4 and 5. Assume now that the leak started two minutes earlier at time 198 minutes, but in section no. 22, i.e. about 250 meters upstream of the original location. The differences in upstream and downstream water level are shown in Figure 15. The difference in the downstream water level is hardly above 0.005 m and there is never more than a difference of 0.009 m in the upstream level. Compared to the natural variations in the water levels as seen in Figure 12 these differences are small.

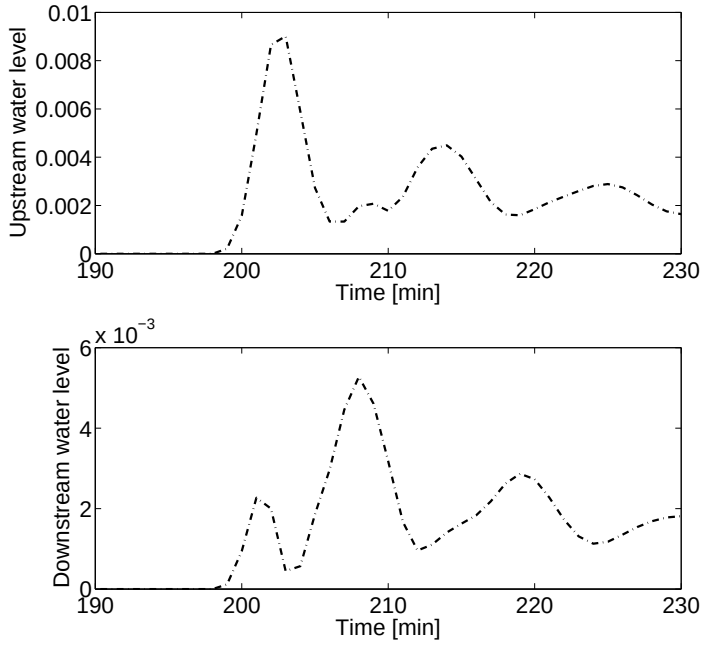

FIGURE 15. Difference in water level for leaks at different locations

The above considerations show that having a good estimate of the start time of a leak can be crucial for successful location of the leak. Also note that data observed after a certain time after the leak occurred carries relatively little information about the location of the leak since the effects are then very similar at the boundaries. Hence, the integration time T should be chosen such that it covers the period when there are relatively large differences but not any longer time period. Moreover the boundary conditions are often at least partially given by a control system which objective is to maintain the water levels at constant setpoints, and this will further mask any difference between leak locations. Due to the uncertainty in the starting time of a leak, the bank of model/observers could be extended to include models/observers where the leak starts at different times.

Furthermore, the above discussion also points to an alternative approach to the leak localization problem. As the velocities λ_+ and λ_- are approximately equal, the time difference between the effect of a leak is seen at the upstream end and the downstream end can be used to estimate the position of the leak. Let $\tau = L/\lambda_+$,

the time it takes to travel the length of the pool. Let δt be the time difference between the effect is seen at the upstream end and the downstream end. If δt is zero we expect the leak to be in the middle, if it is close to $\pm\tau$ we expect it to be at the upstream/downstream end and more generally

$$\hat{x}_l = (1/2 - \delta t/(2\tau)) \cdot L$$

Note that this approach does not rely on having an estimate of the time the leak started as it is solely based on the time difference between the effects can be seen at the upstream and downstream end.

However, it can still be difficult to apply this approach to real data. As an example, Figure 16 shows the upstream and downstream water level in Pool 4 of the Coleambally 6 channel at the time the offtake started. It is not clear when the water levels start decreasing. Taking into account the values of λ_+ and λ_-, an uncertainty of 1 minute in when the effect is seen corresponds to an uncertainty of about 200 m in the position of the leak illustrating the difficulty of the problem.

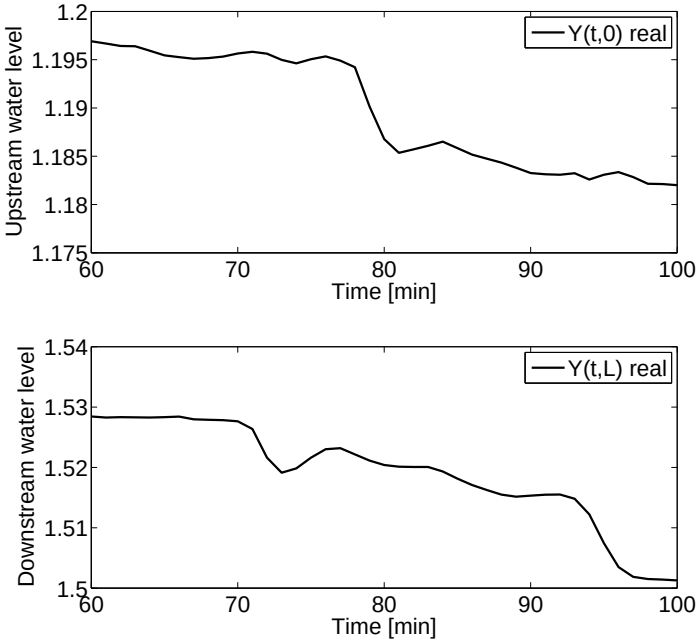

FIGURE 16. Upstream and downstream water level at the time when the leak started

7. **Conclusion.** In this paper, we proposed two methods to estimate the position of a leak in an open-water channel. Both methods work well under ideal conditions and within a range of uncertainties. A heuristic analysis has been presented which shows that the leak localization problem is an inherently difficult problem, and based on the analysis a simplified approach using the time difference between the effects of a leak are seen at the upstream end and the downstream end has been suggested.

REFERENCES

[1] O. M Aamo, J. Salvesen and B. A Foss, "Observer Design Using Boundary Injections for Pipeline Monitoring," International Symposium on advanced control of chemical processes, Gramado, Brazil, 2006.

[2] G. Bastin, J. M. Coron and B. D'Andra-Novel, "Using Hyperbolic Systems of Balance Laws for Modelling, Control and Stability Analysis of Physical Networks," 17th IFAC World Congress, Lecture notes for the Pre-Congress Workshop on Complex Embedded and Networked Control Systems, Seoul, South Korea, July 2008.

[3] N. Bedjaoui, X. Litrico, A. Lourosa and J. R. Bruno, *Application of data reconciliation on an irrigation canal*, 7th conference on Hydroinformatics, **2** (2006), 1503–1510, Nice, France.

[4] N. Bedjaoui, X. Litrico, D. Koenig, P. O. Malaterre and J. R. Bruno, *Static and dynamic data reconciliation for an irrigation canal*, Journal of Irrigation and Drainage, **134** (2009), 778–787.

[5] M. G. Bos (Ed.), "Discharge Measurement Structures," International Institute for Land Reclamation and Improvement/ILRI, Waageningen, The Netherlands, 1978.

[6] M. Cantoni, E. Weyer, Y. Li, S. K. Ooi, I. Mareels and M. Ryan, *Control of large-scale irrigation networks*, IEEE Proceedings special issue on The Emerging Technology of Networked Control Systems, **95** (2007), 75–91.

[7] M. H. Chaudhry, "Open Channel Flow," Prentice Hill, 1993.

[8] J. F. Dulhoste, D. Georges and G. Besancon, *Nonlinear control of open-channel water flow based on collocation control model*, Journal of Hydraulic Engineering, **130** (2004), 254–266.

[9] M. Gomez, J. Rodellar and J. A. Mantecon, *Predictive control method for decentralised operation of irrigation canals*, Applied Mathematical Modelling, **26** (2002), 1039–1056.

[10] J. de Halleux, C. Prieur, J-M Coron, B. d'Andrea-Novel and G. Bastin, *Boundary feedback control in networks of open-channel*, Automatica J. IFAC, **39** (2003), 1365–1376.

[11] Y. Li and M. Cantoni, *Distributed controller design for open water channels*, Proceedings of "17th IFAC World Congress," 10033–10038, Seoul, South Korea, July, (2008).

[12] X. Litrico, V. Fromion, J.-P. Baume, C. Arranja and M. Rijo, *Experimental validation of a methodology to control irrigation canals based on Saint-Venant equations*, Control Engineering Practice, **13** (2005), 1425–1437.

[13] I. Mareels, E. Weyer, S. K. Ooi, M. Cantoni, Y. Li and G. Nair, *Systems engineering for irrigation systems: Success and challenges*, Annual review in control, IFAC, **29** (2005), 191–204.

[14] S. K. Ooi and E. Weyer, *Control design for an irrigation channel form physical data*, Control Engineering Practice, **16** (2008), 1132–1150

[15] C. Prieur, J. Winkin and G. Bastin, *Robust boundary control of systems of conservation laws*, Mathematics of control, signals and Systems, Mathematics of Control, Signals and Systems, **20** (2008), 173–197.

[16] J. Schuurmans, A. Hof, S. Dijkstra, O. H. Bosgra and R. Brouwer, *Simple water level controller for irrigation and drainage canals*, Journal of Irrigation and Drainage Engineering, **125** (1999), 189–195.

[17] E. Weyer, *Control of irrigation channels*, IEEE Transaction on Control System Technology, **16** (2008), 664–675.

[18] E. Weyer and G. Bastin, *Leak detection in open water channel*, Proceedings of "17th IFAC World Congress," 7913–7918, Seoul, South Korea, July, (2008).

Received November 2008; revised January 2009.

E-mail address: n.bedjaoui@ee.unimelb.edu.au
E-mail address: e.weyer@ee.unimelb.edu.au
E-mail address: bastin@inma.ucl.ac.be